Ground- and Excited-State Proton Transfer and Rotamerism in 2-(2-Hydroxyphenyl)-5-phenyl-1,3,4-oxadiazole and Its O/"NH or S"-Substituted Derivatives

Zhenna Yang, Shuangyang Yang, and Jingping Zhang*

Faculty of Chemistry, Northeast Normal University, Changchun 130024, China

Received: December 14, 2006; In Final Form: May 13, 2007

The intramolecular proton-transfer process, rotational process, and optical properties of 2-(2-hydroxyphenyl)-5-phenyl-1,3,4-oxadiazole (HOXD) and its O/"NH"- and O/"S"-substituted derivatives, 2-(2-hydroxyphenyl)-5-phenyl-1,3,4-triazole (HOT) and 2-(2-hydroxyphenyl)-5-phenyl-1,3,4-thiadiazole (HOTD), respectively, have been studied. DFT (B3LYP/6-31+G**) single-point energy calculations were performed using HF- and DFT-optimized geometries in the ground state (S_0). TD-B3LYP/6-31+G** calculations using CIS-optimized geometries were carried out to investigate the properties of the first singlet excited state (S_1) and first triplet excited state (T_1). The computational results revealed that a high-energy barrier inhibits the proton transfer from *cis*-enol (E_c) to keto (K) form in S_0, whereas the proton transfer in S_1 can take place through a very-low-energy barrier. The rotation between E_c and *trans*-enol (E_t) can occur in S_0 through a low-energy barrier, whereas it is prohibited because of the high-energy barrier in S_1 for each of the three molecules. The vertical excitation energies were calculated using the TD-B3LYP/6-31+G** method based on the HF- and CIS-optimized geometries. Absorption and fluorescence wavelengths of HOT show a hypsochromic shift (6−15 nm) relative to HOXD, while those of HOTD show a bathochromic shift (21−29 nm). The phosphorescence wavelength of HOTD shows a significant bathochromic shift relative to that of HOXD.

1. Introduction

The photoinduced excited-state intramolecular proton transfer (ESIPT) process is one of the most fundamental photochemical reactions that has been studied extensively both experimentally and theoretically[1] since the studies of the fluorescence of methyl salicylate by Weller.[1a] Photoexcitations in hydrogen-bonded systems usually lead to significant changes in the electron density of their acidic and basic centers[2−4] that facilitate the transference of the H atom and the formation of phototautomers. The most striking feature of the dynamics in these systems is their ultrafast nature and the highly Stokes-shifted fluorescence of the tautomer produced through the process.[5] The Stokes shift values typical of the phototautomer forms vary in the range of 6000−12 000 cm^{-1} for different ESIPT compounds.

2-(2-Hydroxyphenyl)-5-phenyl-1,3,4-oxadiazole (HOXD) is an example of a molecular system that undergoes ESIPT to yield an excited keto form of the original enol form and emits quite strong ESIPT fluorescence.[6,7] This molecule has been studied widely not only because of its ESIPT character, but also because of the triplet phosphorescence emission of the enol form,[6,7] which raises the electroluminescent efficiency that is required for electroluminescence materials of organic light-emitting diodes (OLEDs) in flat panel display technologies.

Doroshenko et al. performed experimental and theoretical studies of HOXD and its several derivatives to find the substituent effects on the fluorescence properties.[8,9] They optimized the molecular geometry in the ground (S_0) and first excited singlet state (S_1) by the AM1 semiempirical method and calculated the spectral characteristics for AM1-optimized structures using the ZINDO/S scheme.[8,9] However, to the best of our knowledge, no calculation about the T_1 state of HOXD has been reported thus far. In addition, semiempirical methods have limitations, especially for the calculation of the excited state. Recently, Gaenko et al. studied three substituted HOXDs with the substituents being *N*,*N*′-dimethylamino, methoxy, or a phenyl group conducted at the high ab initio level.[10]

In this work, we investigated the intramolecular proton transfer and rotational processes in the ground and excited states (S_1 and T_1). Furthermore, we studied the optical properties at the TD-DFT level. To design new materials with ESIPT character, we performed a theoretical study on O/"NH"- and O/"S"-substituted derivatives, 3-(2-hydroxyphenyl)-5-phenyl-4*H*-1,2,4-triazole (HOT) and 2-(2-hydroxyphenyl)-5-phenyl-1,3,4-thiadiazole (HOTD), to investigate the substituent effects on the intramolecular proton transfer, the rotational processes, and the optical properties. The structures studied in this work are shown in Scheme 1, along with the atom numbering.

2. Computational Methods

All calculations were performed by means of the Gaussian 03 package.[11] The geometry optimization for S_0 was carried out using HF and DFT[12] methods, while the configuration interaction with single excitations (CIS) method[13] was employed to optimize the geometries for the excited states (S_1 and T_1). All geometry optimizations were performed using the 6-31G* basis set. Frequency calculations using the same methods as those for the geometry optimizations were performed for the obtained structures. All real frequencies have confirmed the presence of a local minimum, while one imaginary frequency indicated the existence of a transition state.

To introduce the dynamic electron correlation, single-point energy calculations for the ground and excited states have been

* Corresponding author. E-mail: zhangjingping66@yahoo.com.cn.

10.1021/jp068589x CCC: $37.00
Published on Web 06/21/2007

SCHEME 1: Geometries of *cis*-Enol (E_c), *trans*-Enol (E_t), and Keto (K) Forms of HOXD, HOT, and HOTD, along with Atom Numbering

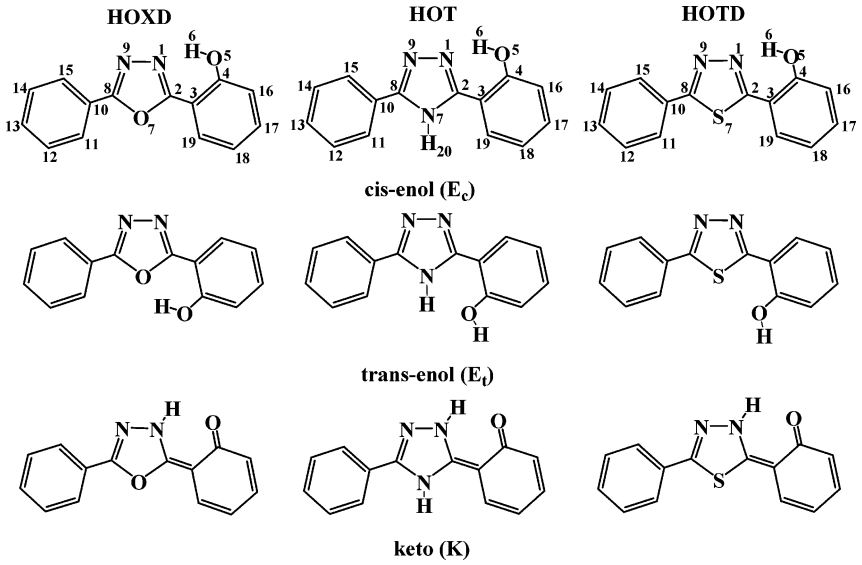

done at the DFT and TD-DFT[14−16] levels, respectively, with B3LYP, Becke's three-parameter functional,[17] and with nonlocal correlation provided by the LYP[18] expression, using the 6-31+G** basis set. Vertical electronic excitation energies were predicted using the TD-B3LYP/6-31+G** method with the ground and excited state optimized geometries, respectively. The hybrid method (denoted as single-point calculation//optimization method) such as DFT//HF or TD-DFT//HF or TD-DFT//CIS has been proved to be an efficient approach in predicting energy parameters[19] or optical properties for LED materials.[20]

The geometry optimizations for the ground and excited states of HOXD were also performed with the Turbomole 5.7[21] program suite at the DFT and TD-DFT levels, respectively, using the B3LYP functional. The TZVP basis set was used for all atoms. The optical properties were also predicted at the TD-B3LYP/TZVP level based on the optimized ground and excited states geometries.

3. Results and Discussion

3.1. Intramolecular Proton Transfer. *3.1.1. Geometrical Parameters*. The main optimized geometric parameters of two tautomers (E_c and K) and transition states (TS) for HOXD, HOT, and HOTD in S_0 (^1E_c, ^{1}TS, ^{1}K), S_1 (^1E_c*, ^{1}TS*, ^{1}K*), and T_1 (^3E_c*, ^{3}TS*, ^{3}K*) are presented in Table 1. HOXD exhibits C_s symmetry in the three states, which was corroborated by the frequency calculation. The geometries of HOT and HOTD were fully optimized without any symmetry constraints. The Cartesian coordinates of E_c, K, and TS of these three molecules for the ground and excited states are given in the Supporting Information. The ground-state geometry optimizations were performed at both HF/6-31G* and B3LYP/6-31G* levels. Comparing the optimized geometries for the ground state at the HF/6-31G* (Table 1) and the B3LYP/6-31G* levels (Table S1 in the Supporting Information), one may find that the hydrogen bond strengths of ^1E_c and ^{1}K for these three molecules at the B3LYP level are stronger than those at the HF level, especially for ^{1}K. For ^1E_c, the B3LYP-optimized $N_1\cdots H_6$ and $N_1\cdots O_5$ distances are shorter by 0.12−0.13 Å and 0.06−0.07 Å, respectively, whereas the O_5-H_6 distance is elongated by 0.03−0.04 Å and θ ($N_1H_6O_5$) is increased by 4° when compared to the corresponding values calculated at the HF level. The discrepancy is more remarkable for ^{1}K, where the $O_5\cdots H_6$ and $N_1\cdots O_5$ distances are decreased by 0.21−0.22 and 0.07 Å, whereas the N_1-H_6 distance and θ ($N_1H_6O_5$) are increased by 0.04−0.05 Å and 9−10°, respectively, at the B3LYP level. Our results confirm the previous report that the B3LYP method overestimates the strength of hydrogen bonds.[22]

According to Brillouin's theorem,[23] CIS calculations of the excited state are the equivalent of a HF calculation for the ground state; therefore, we only list HF-optimized geometries in Table 1. Comparing the geometrical parameters involved in the intramolecular hydrogen bond of the E_c form of the three molecules in each state, we can find that the difference of the O_5-H_6 distance is negligible (<0.003 Å), while the $N_1\cdots H_6$ and $N_1\cdots O_5$ distances are shorter and θ ($N_1H_6O_5$) is slightly larger in the derivatives than those of HOXD (Table 1). As a consequence, the hydrogen bond strength of E_c gets stronger in the derivatives for each of the three states. The most prominent difference in the geometries of the transition states is the decrease in the interatomic distances between heavy atoms ($N_1\cdots O_5$) and the increase of θ ($N_1H_6O_5$) in each state of the three molecules. The shortest $N_1\cdots O_5$ distance and largest θ ($N_1H_6O_5$) values are found in TS among three forms (E_c, TS, K). The increasing hydrogen bond strength in TS should facilitate the intramolecular proton transfer from E_c to K.

3.1.2. Frontier Molecular Orbitals. The origin of the geometric difference introduced by excitation can be explained, at least in qualitative terms, by analyzing the change in the bonding character of the orbitals involved in the electronic transition for each pair of bonded atoms.[24] An electronic excitation results in some electron density redistribution that affects the molecular geometry. When the HOMO → LUMO transition involves the loss of the bonding character of a bond, the bond concerned is lengthened and vice versa. In all cases, both the HOMO and LUMO have π character. The qualitative molecular orbital representations of the HOMO and LUMO for the ^1E_c, ^1E_c*, ^3E_c*, ^{1}K, ^{1}K*, and ^{3}K* forms of HOXD are shown in Figure 1. The FMOs for HOT and HOTD can be found in the Supporting Information (Figure S1). The $S_0 \rightarrow S_1$ excitation process can be mainly assigned to the HOMO → LUMO transition, which corresponds to a $\pi-\pi$* excited singlet state. The contribution of the HOMO → LUMO transition to the S_1 state is 90, 89, and 90% for ^1E_c of HOXD, HOT, and HOTD, respectively. The distribution patterns of the FMOs are similar in S_0, S_1, and

TABLE 1: Main Geometrical Parameters (Bond Lengths and Angles in Angstroms and Degrees, Respectively) for the Three Stationary Points (E_c, TS, K) of HOXD, HOT, and HOTD in the S_0, S_1, and T_1 States

	HOXD			HOT			HOTD		
	^1E_c	^{1}TS	^{1}K	^1E_c	^{1}TS	^{1}K	^1E_c	^{1}TS	^{1}K
N_1-C_2	1.274	1.293	1.320	1.290	1.303	1.323	1.281	1.302	1.329
C_2-C_3	1.458	1.419	1.384	1.468	1.437	1.409	1.469	1.428	1.390
C_3-C_4	1.400	1.427	1.451	1.401	1.424	1.445	1.403	1.429	1.457
C_4-O_5	1.333	1.273	1.230	1.331	1.277	1.235	1.331	1.273	1.229
O_5-H_6	0.956	1.329	1.980	0.959	1.311	1.925	0.957	1.304	1.869
N_1-H_6	1.938	1.160	1.001	1.879	1.168	1.003	1.879	1.167	1.005
N_1-O_5	2.745	2.366	2.607	2.699	2.368	2.595	2.693	2.370	2.592
$N_1H_6O_5$	140.6	143.8	118.2	141.8	145.4	121.6	141.2	147.1	126.1
	HOXD			HOT			HOTD		
	^1E_c*	^{1}TS*	^{1}K*	^1E_c*	^{1}TS*	^{1}K*	^1E_c*	^{1}TS*	^{1}K*
N_1-C_2	1.334	1.323	1.336	1.349	1.334	1.344	1.352	1.343	1.345
C_2-C_3	1.399	1.392	1.395	1.404	1.397	1.403	1.409	1.403	1.413
C_3-C_4	1.440	1.499	1.495	1.439	1.499	1.499	1.439	1.483	1.494
C_4-O_5	1.326	1.267	1.230	1.325	1.268	1.229	1.322	1.267	1.230
O_5-H_6	0.957	1.240	2.089	0.959	1.222	2.070	0.960	1.231	1.941
N_1-H_6	1.925	1.239	0.998	1.894	1.251	0.997	1.859	1.237	1.003
N_1-O_5	2.739	2.378	2.664	2.715	2.378	2.665	2.683	2.381	2.637
$N_1H_6O_5$	141.4	147.2	114.6	142.0	148.3	116.2	142.2	149.5	124.05
	HOXD			HOT			HOTD		
	^3E_c*	^{3}TS*	^{3}K*	^3E_c*	^{3}TS*	^{3}K*	^3E_c*	^{3}TS*	^{3}K*
N_1-C_2	1.292	1.314	1.353	1.302	1.317	1.353	1.347	1.326	1.370
C_2-C_3	1.447	1.404	1.356	1.461	1.428	1.370	1.432	1.403	1.369
C_3-C_4	1.404	1.433	1.470	1.403	1.427	1.463	1.418	1.441	1.482
C_4-O_5	1.331	1.269	1.212	1.330	1.274	1.213	1.332	1.267	1.212
O_5-H_6	0.956	1.298	2.202	0.959	1.291	2.153	0.955	1.275	2.084
N_1-H_6	1.933	1.180	0.992	1.874	1.181	0.992	1.902	1.188	0.993
N_1-O_5	2.739	2.365	2.729	2.692	2.366	2.718	2.711	2.371	2.707
$N_1H_6O_5$	140.4	145.3	111.7	141.6	146.3	114.4	141.0	148.4	118.9

T_1 for each tautomer. The distribution of HOMO on phenyl ring increases in the sequence $T_1 > S_1 > S_0$ for E_c forms, while the distribution of LUMO on phenolic ring increases in the sequence $T_1 > S_1 > S_0$ for K forms.

The distribution patterns of the HOMO and LUMO also provide a remarkable signature for the charge-transfer character of the transition. It can be seen from Figure 1 that the excitation of the electron from the HOMO to the LUMO leads to the electronic density flow mainly from the phenol ring to the heterocycle in the E_c form and from the phenolic ring to the protonated heterocycle and the benzene ring in the K form. This is consistent with the results of Doroshenko et al.[8,9] The distribution patterns of FMOs in the S_1 (T_1) state for E_c* and K* tautomers suggest a stronger charge-transfer character for ^{3}K* (^{1}K*) than that of ^3E_c* (^1E_c*). The structures of the HOMO and LUMO of all three molecules are almost the same (Figures 1 and S1), and therefore they should have similar charge-transfer character. For the E_c form, the changes in the electronic density result in an increase in the acidity of the hydroxy group and the basicity of the oxadizole ring, which favors the proton transfer from the enol form to the keto form in S_1. There will be an increase in the acidity of the protonated heterocycle and basicity of the phenolic ring after the relaxation of the K form from S_1 to S_0 through fluorescent emission. This favors the reverse proton transfer from ^{1}K to the starting ^1E_c in S_0 to finish the cyclic four-level photophysical scheme ($^1E_c \rightarrow {}^1E_c$* $\rightarrow {}^1$K* $\rightarrow {}^1$K $\rightarrow {}^1E_c$).

3.1.3. Energy Parameters. The energy difference (ΔE) between E_c and K (positive value indicates that E_c is more stable than K), the direct ($\Delta E_d^{\#}$), and reverse ($\Delta E_r^{\#}$) energy barriers for the proton transfer of the three molecules in S_0, S_1, and T_1 states are listed in Table 2. The ground-state calculations are carried out at the HF/6-31+G**//HF/6-31G*, B3LYP/6-31+G**//HF/6-31G*, and B3LYP/6-31+G**//B3LYP/6-31G* levels. It is shown in Table 2 that ^1E_c is much more stable than ^{1}K, which is ascribed to the existence of the aromatic phenol ring in ^1E_c that is not present in ^{1}K.[25] This can be found from the HF/6-31G*-optimized geometrical parameters where the difference between the longest and shortest C−C distances in the $C_3C_4C_{16}C_{17}C_{18}C_{19}$ ring is 0.026 Å (0.109 Å), 0.026 Å (0.101 Å), and 0.030 Å (0.113 Å), respectively, for ^1E_c (^{1}K) of HOXD, HOT, and HOTD. It is worth noting that the proton transfer in S_0 involves a higher $\Delta E_d^{\#}$ because of the loss of aromaticity along this process for each compound. The calculated energy parameters (ΔE, $\Delta E_d^{\#}$, $\Delta E_r^{\#}$) at the HF/6-31+G**//HF/6-31G* level are higher than those obtained at the other two levels, especially for $\Delta E_d^{\#}$ or $\Delta E_r^{\#}$. This is because the HF method is known to overestimate the energy barriers in reactions.[19] The calculated values for ΔE, $\Delta E_d^{\#}$, and $\Delta E_r^{\#}$ at the B3LYP/6-31+G**//HF/6-31G* level are close to those obtained at the B3LYP/6-31+G**//B3LYP/6-31G* level, which was also reported in a previous article.[19] The ΔE values calculated at the former level are slightly higher than those obtained at the latter one by less than 1 kcal/mol, while energy barriers ($\Delta E_d^{\#}$ and $\Delta E_r^{\#}$) at the latter level are more positive by 0.8−2.1 kcal/mol. Furthermore, the less negative values of $\Delta E_r^{\#}$ (absolute value less than 2.02 and 0.23 kcal/mol for B3LYP/ 6-31+G**//HF/6-31G* and B3LYP/6-31+G**//B3LYP/6-31G*, respectively) suggest that the B3LYP method slightly underestimates the energy barriers of the proton-transfer process. It was also recently reported that the B3LYP method provides negative energy barriers for radical addition reaction.[26] The large endothermicity and high $\Delta E_d^{\#}$ impose a restriction on the occurrence of the proton transfer in S_0 for each compound.

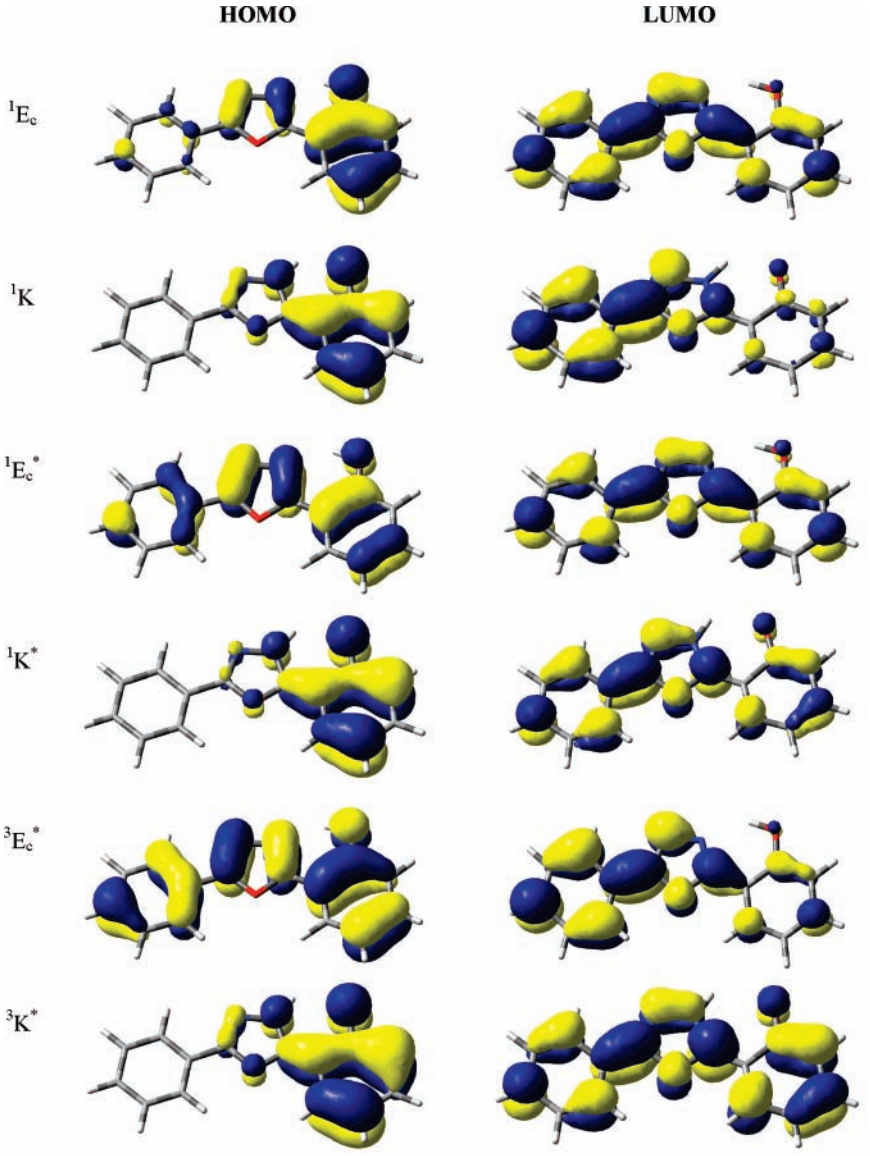

Figure 1. HOMO and LUMO for the *cis*-enol (^1E_c, ^1E_c*, ^3E_c*) and keto (^1K, ^1K*, ^3K*) tautomers of HOXD.

TABLE 2: Energy Difference (ΔE) between E_c and K and Direct ($\Delta E_d^{\#}$) and Reverse ($\Delta E_r^{\#}$) Energy Barriers for the Proton Transfer of HOXD, HOT, and HOTD in the S_0, S_1, and T_1 States (kcal/mol)

	HOXD			HOT			HOTD		
	ΔE	$\Delta E_d^{\#}$	$\Delta E_r^{\#}$	ΔE	$\Delta E_d^{\#}$	$\Delta E_r^{\#}$	ΔE	$\Delta E_d^{\#}$	$\Delta E_r^{\#}$
S_0[a]	16.42	22.10	5.67	12.77	18.08	5.31	13.94	18.45	4.51
S_0[b]	13.18	11.74	−1.43	10.82	9.50	−1.32	11.50	9.48	−2.02
S_0[c]	13.06	13.12	0.06	10.15	10.88	0.73	10.53	10.29	−0.23
S_1	−6.00	2.13	8.13	−8.34	0.88	9.22	−4.93	0.01	4.94
T_1	0.38	7.08	6.69	−2.45	5.09	7.54	2.09	7.02	4.92

[a] HF/6-31+G**//HF/6-31G*. [b] B3LYP/6-31+G**//HF/6-31G*. [c] B3LYP/6-31+G**//B3LYP/6-31G*.

However, the reverse proton reaction will occur easily through a very-low-energy barrier (at least lower than the HF predicted values in the range 4.51−5.67 kcal/mol) or a barrierless process.

One can see from the TD-B3LYP/6-31+G**//CIS/6-31G* results in Table 2 that the endothermic proton-transfer process in S_0 becomes an exothermic one in S_1, whereas the direct energy barriers decrease substantially in comparison with the S_0 state for the three molecules. A reverse of the stability of enol and keto tautomers was also pointed out in the analysis of the $^1\pi\pi^*$ excitation in intramolecular hydrogen-bonded systems having a phenol ring.[27−29] Comparing the HF/6-31G*- and CIS/6-31G*-optimized geometrical parameters, we can find that the difference between the longest and shortest distances in the $C_3C_4C_{16}C_{17}C_{18}C_{19}$ ring is 0.074, 0.071, and 0.073 Å, respectively, for ^1E_c* of HOXD, HOT, and HOTD, in comparison with S_0 (where this difference equals 0.026, 0.026, and 0.030 Å, respectively), indicating the loss of aromaticity in the excitation process, which favors the ESIPT reaction. Both the ΔE and $\Delta E_r^{\#}$ values for HOXD in the S_1 state are lower than those of HOT, but larger than the corresponding ones of HOTD. The $\Delta E_d^{\#}$ values are in the following order: HOXD > HOT > HOTD. The proton-transfer process of HOTD is almost barri-

TABLE 3: Energy Difference between E_c and E_t (ΔE), the Direct ($\Delta E_d^{\#}$), and Reverse ($\Delta E_r^{\#}$) Energy Barriers for the Rotational Process in the Ground and Excited States (kcal/mol)

	HOXD			HOT			HOTD		
	ΔE	$\Delta E_d^{\#}$	$\Delta E_r^{\#}$	ΔE	$\Delta E_d^{\#}$	$\Delta E_r^{\#}$	ΔE	$\Delta E_d^{\#}$	$\Delta E_r^{\#}$
S_0	5.75	11.26	5.51	4.44	10.28	5.83	7.46	10.53	3.07
S_1	6.79	23.73	16.93	6.93	25.63	18.71	10.74	18.24	7.50
T_1	4.02	17.90	13.88	4.89	14.33	9.44	7.36	17.22	9.86

TABLE 4: Computed Absorption (λ_{abs}), Fluorescence (λ_{fl}), and Phosphorescence (λ_{ph}) Wavelengths (nm) of HOXD, HOT, and HOTD, along with Available Experimental Data of HOXD[a]

	λ_{abs}	λ_{fl}	λ_{ph}
HOXD	272.27 (4.55), 309.00 (4.01)	360.99 (3.43), 471.35 (2.63)	543.69 (2.28), 481.95 (2.57)[b]
HOT	264.90 (4.68), 302.23 (4.10)	347.14 (3.57), 465.97 (2.66)	
HOTD	293.97 (4.22), 338.34 (3.66)	386.28 (3.21), 497.28 (2.49)	663.12 (1.87), 582.95 (2.13)[b]
Exp[c]	275 (4.51),[d] 315 (3.94)[d]	370 (3.35),[d] 475 (2.61)[d]	
	274 (4.53),[e] 315 (3.94)[e]	365 (3.40),[e] 489 (2.54)[e]	481 (2.58)[e]

[a] The values in parentheses are the transition energies (in electronvolts) corresponding to the wavelengths listed. [b] Computational results at the B3LYP/6-31+G** level. [c] Exp = Experimental values of HOXD. [d] Data from ref 6. [e] Data from ref 7.

erless. For each of the three molecules, the ESIPT process can take place easily through a lower energy barrier in S_1, resulting in larger rate constants.

Experimentally,[6,7] only the enol phosphorescence can be observed for HOXD. Thus, HOXD belongs to the first triplet state potential case proposed by Kasha et al.[30] In T_1, the calculated result shows that ^3E_c* is slightly more stable than ^3K* (by 0.38 kcal/mol), in accordance with the experimental result. For HOT, the energy of ^3E_c* is higher than that of ^3K* by 2.45 kcal/mol. ^3K* can hardly undergo the reverse proton transfer, and the chance to observe the phosphorescence of ^3K* is rare.[30] For HOTD, ^3E_c* is also more stable than ^3K* (by 2.09 kcal/mol). Therefore, only the enol phosphorescence should be observed, making HOTD a good candidate as the organic light-emitting materials for the phosphorescence emission. The $\Delta E_r^{\#}$ value of HOTD is ca. 1.8 kcal/mol lower than that of HOXD, yielding an easier reverse proton-transfer reaction in HOTD.

The ground- and excited-state geometry optimizations of E_c and K for HOXD were also performed at the B3LYP/TZVP and TD-B3LYP/TZVP levels, respectively. The energy parameters are given in the Supporting Information (Table S2). In S_0, E_c is more stable than K by 12.96 kcal/mol. In S_1 and T_1, K is more stable than E_c by 11.11 and 1.05 kcal/mol, respectively. Obviously, the TD-B3LYP/TZVP method fails to provide a correct energy ordering with the available experimental result for the T_1 state of HOXD. This is because the TD-B3LYP/TZVP method underestimates the relative stability of the E_c form for HOXD in T_1. It was also found that the TD-DFT method systematically underestimates the energy of charge-transfer excited states.[31] For HOXD, the charge-transfer characteristic of the ^3K* is more significant than that of the ^3E_c*. Perhaps this is why the TD-B3LYP/TZVP method overestimates the stability of the keto form for HOXD in T_1. Therefore, we did not perform further calculations for HOT and HOTD at the B3LYP/TZVP or TD-B3LYP/TZVP level.

3.2. Rotational Process. In Table 3, we listed the energy difference between E_c and E_t (positive value indicates that E_c is more stable than E_t), the direct and reverse energy barriers for the rotational process. The calculations were performed at the B3LYP/6-31+G**//HF/6-31G* level for S_0 and the TD-B3LYP/6-31+G**//CIS/6-31G* level for S_1 and T_1. The Cartesian coordinates of E_t (^1E_t, ^1E_t*, ^3E_t*) and TS of the rotational process (^1TS_r, ^1TS_r*, ^3TS_r*) of the three compounds in the S_0, S_1, and T_1 states are presented in the Supporting Information. The schematic energy diagrams of the three compounds are shown in the Supporting Information (Figure S2). In S_0, for each compound, E_t is more stable than K, while the stability of the two forms is inverted in S_1 and T_1. The direct and reverse energy barriers of the rotational process are higher than those of the proton-transfer process in S_1 and T_1.

In S_0, the energy ordering is as following: $^1K > {}^1E_t > {}^1E_c$ for each of the three compounds (Figure S2), implying that ^1E_c should be the most abundant and stable species. In S_0, the energy of ^1E_t is higher than that of ^1E_c by 5.75 kcal/mol and the $\Delta E_d^{\#}$ and $\Delta E_r^{\#}$ are 11.26 and 5.51 kcal/mol for HOXD. Because of the repulsion between sulfur and hydrogen, the dihedral of $H_6O_5C_4C_3$ for ^1E_t of HOTD tends to 180° (Scheme 1). Both the $\Delta E_d^{\#}$ and $\Delta E_r^{\#}$ of HOTD (10.53 and 3.07 kcal/mol) are lower than those of HOXD. The direct energy barrier of HOT is lower than that of HOXD by 0.98 kcal/mol, while the reverse energy barrier is slightly higher than that of HOXD by 0.32 kcal/mol. The rotation between ^1E_c and ^1E_t can occur through the low-energy barriers in S_0 at room temperature for the three compounds.

In S_1, the endothermicity is increased by 1−3 kcal/mol relative to that of S_0, whereas the $\Delta E_d^{\#}$ and $\Delta E_r^{\#}$ values of HOXD (23.73 and 16.93 kcal/mol), HOT (25.63 and 18.71 kcal/mol), and HOTD (18.24 and 7.50 kcal/mol) are about one or two times higher than their corresponding values in S_0. The high-energy barriers inhibit the rotation between ^1E_c* and ^1E_t* in S_1. In T_1, ^3E_c* is more stable than ^3E_t* by 4.02, 4.89, and 7.36 kcal/mol for HOXD, HOT, and HOTD, respectively. Both $\Delta E_d^{\#}$ and $\Delta E_r^{\#}$ of HOXD and HOT and $\Delta E_d^{\#}$ of HOTD are higher than the corresponding values in S_0, while lower than the values in S_1. The $\Delta E_r^{\#}$ of HOTD in T_1 is the largest one among the three states.

3.3. Electronic Transition. The calculated vertical excitation energies by the TD-B3LYP/6-31+G** approach using the HF/6-31G*- and CIS/6-31G*-optimized geometries are summarized in Table 4. The long-wavelength and short-wavelength absorption correspond to the excitation of ^1E_c to the first and second excited singlet states (S_1 and S_2). The two excited states (S_1 and S_2) can be mainly assigned to HOMO → LUMO and HOMO−1 → LUMO transition. After the photoexcitation of the ^1E_c form to the lowest excited singlet state ^1E_c*, ultrafast singlet proton transfer will take place and proton photo transfer efficiency is close to 100%. Thus, its contribution to the normally Stokes-shifted emission is negligible and the short-wavelength emission band belongs to the emission of ^1E_t*. The long-wavelength emission band characterized by high Stokes shift values is attributed to the emission of ^1K* formed by ESIPT ($^1E_c \rightarrow {}^1E_c^* \rightarrow {}^1TS^* \rightarrow {}^1K^* \rightarrow {}^1K$). Therefore, the short-

TABLE 5: Energies for HOMO and LUMO and the Energy Gap (E_g) for ^1E_c, ^1E_t, ^1E_t*, ^1K*, and ^3E_c* of HOXD, HOT, and HOTD (eV)

	HOXD			HOT			HOTD		
	HOMO	LUMO	E_g	HOMO	LUMO	E_g	HOMO	LUMO	E_g
^1E_c	−6.50	−1.96	4.54	−6.18	−1.59	4.59	−6.32	−2.17	4.15
^1E_t	−6.45	−1.88	4.57	−6.09	−1.35	4.74	−6.29	−1.85	4.44
^1E_t*	−6.01	−2.30	3.71	−5.57	−1.74	3.83	−5.74	−2.29	3.45
^1K*	−5.29	−2.26	3.03	−5.07	−1.99	3.08	−5.34	−2.55	2.79
^3E_c*	−6.14	−2.32	3.82				−5.96	−2.62	3.34

wavelength and long-wavelength fluorescence emissions are calculated using the optimized geometries of ^1E_t* and ^1K*, respectively. ^1K* can also transit to ^3K* through the intersystem crossing. For molecules with ESIPT property, it was found that the ESIPT facilitates the intersystem crossing.[30] Subsequently, if ^3E_c* is more stable than ^3K*, it will be created via the reverse proton transfer from ^3K*. Eventually, phosphorescence of ^3E_c* will be observed ($^1K^* \rightarrow {}^3K^* \rightarrow {}^3TS^* \rightarrow {}^3E_c^* \rightarrow {}^1E_c$).[30] Phosphorescence emission energies of HOXD and HOTD are calculated using the optimized geometries of ^3E_c*. For HOT, ^3K* is more stable than ^3E_c* and the chance to observe the phosphorescence of the ^3K* is rare.[30]

The TD-B3LYP/6-31+G** method provides very good prediction for λ_{abs} and λ_{fl}, and the results are in excellent agreement with the absorption and photoluminescence spectrum of HOXD film[6] (deviation within 6 and 9 nm, respectively) or in CH_2Cl_2 solution[7] (deviation within 6 and 18 nm, respectively). The TD-B3LYP/6-31+G** calculated λ_{abs} values of HOXD based on the B3LYP/6-31G*-optimized geometry of ^1E_c are 287.96 and 328.77 nm (deviation within 14 nm), which are in worse accordance with the experimental data than the results obtained at the HF/6-31G*-optimized geometry. The discrepancy may be ascribed to the overestimation of hydrogen bond strength at the DFT level.[22] The TD-B3LYP/6-31+G**//HF/6-31G* maximum absorption wavelengths of ^1E_t of HOXD, HOT, and HOTD are 303.55, 288.99, and 311.06 nm, respectively, which lie at shorter wavelength than those of ^1E_c (309.00, 302.23, and 338.34 nm for HOXD, HOT, and HOTD, respectively). The λ_{abs} and λ_{fl} of HOT and HOTD show hypsochromic (6−15 nm) and bathochromic shifts (21−29 nm) relative to those of HOXD. Thus, O/"S" substitution has a more pronounced influence on λ_{abs} of ^1E_c and λ_{fl} of ^1E_t* and ^1K*, while O/"NH" substitution has a more significant effect on λ_{abs} of ^1E_t. The effect of the substitution on optical properties can be explained from the energies of HOMO and LUMO involved in the excitation (Table 5). The results are obtained using the TD-B3LYP/6-31+G** method based on HF/6-31G* (CIS/6-31G*)-optimized geometries of ^1E_c and ^1E_t (^1E_t*, ^1K*, and ^3E_c*). It is shown in Table 5 that the HOMO−LUMO energy gaps (E_g) of ^1E_c, ^1E_t, ^1E_t*, and ^1K* for HOT (HOTD) are larger (smaller) than those of HOXD. This corresponds to the hypsochromic shift of the λ_{abs} and λ_{fl} of HOT and bathochromic shift of the λ_{abs} and λ_{fl} of HOTD. The E_g difference (ΔE_g) between HOTD and HOXD is 0.39 eV for ^1E_c, 0.26 eV for ^1E_t*, and 0.24 eV for ^1K*. These values are much larger than those predicted between HOT and HOXD (0.05, 0.12, and 0.05 eV for ^1E_c, ^1E_t*, and ^1K*, respectively). This is why the O/"S" substitution shows a more pronounced influence on λ_{abs} of ^1E_c and λ_{fl} of ^1E_t* and ^1K*. The calculated ΔE_g between ^1E_t of HOT and HOXD (0.17 eV) is larger than the one between HOTD and HOXD (0.13 eV), and hence the O/"NH" substitution shows a more significant influence on λ_{abs} of ^1E_t.

The λ_{abs} values at the TD-B3LYP/TZVP level based on B3LYP/TZVP-optimized geometry of ^1E_c for HOXD are 284.61 and 325.64 nm. Compared with the experimental values (Table 4), the TD-B3LYP/TZVP//B3LYP/TZVP method provides slightly better computational results for λ_{abs} values (deviation within 11 nm) than those obtained by TD-B3LYP/6-31+G**//B3LYP/6-31G* (deviation within 14 nm). TD-B3LYP/6-31+G**//HF/6-31G* provides the most accurate λ_{abs} values (deviation within 6 nm). The λ_{abs} of ^1E_t calculated at the TD-B3LYP/TZVP//B3LYP/TZVP level is 318.37 nm, which still lies at shorter wavelength than that of ^1E_c at the same computational level. To obtain the λ_{fl} values of ^1E_t* and ^1K* for HOXD, we also optimized their geometries at the TD-B3LYP/TZVP level. The λ_{fl} values of ^1E_t* and ^1K* for HOXD at the TD-B3LYP/TZVP level are 366.00 and 553.09 nm, respectively. Compared with the experimental results (Table 4), we can find that the λ_{fl} of ^1E_t* is well reproduced; however, the computational value of λ_{fl} for ^1K* is in worse agreement with experimental values. Apparently, the TD-B3LYP/6-31+G**//CIS/6-31G* method provides better prediction for the λ_{fl} of ^1K* for HOXD as well. Hence, we did not perform the calculations for λ_{abs} and λ_{fl} values for the two derivatives at the TD-B3LYP/TZVP level.

It can be seen from Table 4 that the TD-B3LYP method underestimates the phosphorescence excitation energy by 0.3 eV for HOXD. It is a known fact that TD-DFT underestimates excitation energies especially when the excitation is accompanied by charge transfer.[32] However, the calculated result at the B3LYP level (481.95 nm) is in excellent accordance with the experimental value (481 nm). We directly take the B3LYP/6-31+G** energy difference between T_1 and S_0 as the phosphorescence excitation energy, based on the CIS/6-31G*-optimized structure for T_1. The λ_{ph} of HOTD shows a large bathochromic shift relative to that of HOXD, either at the TD-DFT (119 nm) or DFT (101 nm) level. Although TD-B3LYP/6-31+G** λ_{ph} is not in a good quantitative agreement with the experimental result for HOXD, useful trends still can be extracted from the computed phosphorescence wavelengths for HOXD and HOTD. The predicted E_g for ^3E_c* of HOTD is 0.48 eV smaller than that of HOXD (Table 5), and the larger ΔE_g corresponds to a larger bathochromic shift of λ_{ph} compared with λ_{abs} and λ_{fl}. The λ_{ph} at the TD-B3LYP/TZVP level for HOXD (669.41 nm) is obviously in much worse agreement with the experimental value (481 nm) than either the TD-B3LYP/6-31+G**//CIS/6-31G* (543.69 nm) or B3LYP/6-31+G** result (481.95 nm). Thus, we did not calculate the λ_{ph} of HOT and HOTD at the TD-B3LYP/TZVP level.

4. Conclusion

In this article, we investigated the tautomerization and rotation of 2-(2-hydroxyphenyl)-5-phenyl-1,3,4-oxadiazole (HOXD) and its O/"NH" (HOT) and O/"S" (HOTD) substituted derivatives for S_0, S_1, and T_1 states. It was revealed that tautomerization from the *cis*-enol form to keto form is very unlikely in S_0 but energetically favored in S_1, and the direct energy barriers are in the following order: HOXD > HOT > HOTD. The reverse proton transfer can occur in T_1 for HOXD and HOTD, and

O/"S" substitution decreases the reverse energy barrier. The rotation process from ^1E_c to ^1E_t is feasible in S_0, while impossible in S_1 because of the high-energy barriers for each of the three investigated molecules. The optical properties were investigated by the TD-DFT approach, and the TD-B3LYP/6-31+G** method provides excellent agreement with experimental results for absorption and fluorescence wavelengths of HOXD, while it underestimates the phosphorescence excitation energy. The phosphorescence excitation energy obtained by the energy difference between T_1 and S_0 at the B3LYP/6-31+G** level based on the CIS/6-31G*-optimized structure for T_1 is in good accordance with the experimental value. Absorption and fluorescence emission wavelengths of HOT show a hypsochromic shift, while those of HOTD show a bathochromic shift relative to HOXD. Furthermore, the O/"S" substitution shows a more pronounced influence on λ_{abs} of ^1E_c and λ_{fl} of ^1E_t* and ^1K*, while the O/"NH" substitution has a more significant influence on λ_{abs} of ^1E_t. The O/"S" substitution has a more remarkable influence on the λ_{ph} than λ_{abs} and λ_{fl}, and a 101-nm red shift for phosphorescence was predicted for HOTD compared with HOXD at the B3LYP/6-31+G** level.

Acknowledgment. Financial support from the NSFC (No. 50473032) and NCET-06-0321 is gratefully acknowledged.

Supporting Information Available: Cartesian coordinates of the relevant structures; summary of the computational results not given in this text, including stationary points, figures of FMOs, a schematic energy diagram, and tables of geometrical parameters and energies. This material is available free of charge via the Internet at http://pubs.acs.org.

References and Notes

(1) (a) Weller, A. *Z. Elektrochem.* **1956**, *60*, 1144. (b) Sengupta, P. K.; Kasha, M. *Chem. Phys. Lett.* **1979**, *68*, 382. (c) McMorrow, D.; Kasha, M. *J. Am. Chem. Soc.* **1984**, *88*, 2235. (d) Schwartz, B. J.; Peteanu, L. A.; Harris, C. B. *J. Phys. Chem.* **1992**, *96*, 3591. (e) Lahmani, F.; Zehnacker-Rentien, A. *J. Phys. Chem. A* **1997**, *101*, 6141.

(2) Douhal, A.; Lahmani, F.; Zehnacker-Rentien, A. *Chem. Phys.* **1993**, *178*, 493.

(3) Bosch, E.; Moreno, M.; Lluch, J. M. *Chem. Phys.* **1992**, *159*, 99.

(4) Douhal, A.; Lahmani, F.; Zewail, A. H. *Chem. Phys.* **1996**, *207*, 477.

(5) Caldin, E. F.; Gold, V. *Proton-Transfer Reactions;* Chapman and Hall: London, 1975.

(6) Ma, D. G.; Liang, F. S.; Wang, L. X.; Lee, S. T.; Hung, L. S. *Chem. Phys. Lett.* **2002**, *358*, 24.

(7) Liang, F. S.; Wang, L. X.; Ma, D. G.; Jing, X. B.; Wang, F. S. *Appl. Phys. Lett.* **2002**, *81*, 4.

(8) Doroshenko, A. O.; Posokhov, E. A.; Verezubova, A. A.; Ptyagina, L. M. *J. Phys. Org. Chem.* **2000**, *13*, 253.

(9) Doroshenko, A. O.; Posokhov, E. A.; Verezubova, A. A.; Ptyagina, L. M.; Skripkina, V. T.; Shershukov, V. M. *Photochem. Photobiol. Sci.* **2002**, *1*, 92.

(10) Gaenko, A. V.; Devarajan, A.; Tselinskii, I. V.; Ryde, U. *J. Phys. Chem. A* **2006**, *110*, 7935.

(11) Frisch, M. J.; Trucks, G. W.; Schlegel, H. B.; Scuseria, G. E.; Robb, M. A.; Cheeseman, J. R.; Montgomery, J. A., Jr.; Vreven, T.; Kudin, K. N.; Burant, J. C.; Millam, J. M.; Iyengar, S. S.; Tomasi, J.; Barone, V.; Mennucci, B.; Cossi, M.; Scalmani, G.; Rega, N.; Petersson, G. A.; Nakatsuji, H.; Hada, M.; Ehara, M.; Toyota, K.; Fukuda, R.; Hasegawa, J.; Ishida, M.; Nakajima, T.; Honda, Y.; Kitao, O.; Nakai, H.; Klene, M.; Li, X.; Knox, J. E.; Hratchian, H. P.; Cross, J. B.; Adamo, C.; Jaramillo, J.; Gomperts, R.; Stratmann, R. E.; Yazyev, O.; Austin, A. J.; Cammi, R.; Pomelli, C.; Ochterski, J. W.; Ayala, P. Y.; Morokuma, K.; Voth, G. A.; Salvador, P.; Dannenberg, J. J.; Zakrzewski, V. G.; Dapprich, S.; Daniels, A. D.; Strain, M. C.; Farkas, O.; Malick, D. K.; Rabuck, A. D.; Raghavachari, K.; Foresman, J. B.; Ortiz, J. V.; Cui, Q.; Baboul, A. G.; Clifford, S.; Cioslowski, J.; Stefanov, B. B.; Liu, G.; Liashenko, A.; Piskorz, P.; Komaromi, I.; Martin, R. L.; Fox, D. J.; Keith, T.; Al-Laham, M. A.; Peng, C. Y.; Nanayakkara, A.; Challacombe, M.; Gill, P. M. W.; Johnson, B.; Chen, W.; Wong, M. W.; Gonzalez, C.; Pople, J. A. *Gaussian 03*, revision B03; Gaussian, Inc.: Pittsburgh, PA, 2003.

(12) Parr, R. G.; Yang W. *Density-functional theory of atoms and molecules;* Oxford University Press: Oxford, 1989.

(13) Foresman, J. B.; Head-Gordon, M.; Pople, J. A.; Frisch, M. J. *J. Phys. Chem.* **1992**, *96*, 135.

(14) Stratmann, R. E.; Scuseria, G. E.; Frisch, M. J. *J. Chem. Phys.* **1998**, *109*, 8218.

(15) Bauernschmitt, R.; Ahlrichs, R. *Chem. Phys. Lett.* **1996**, *256*, 454.

(16) Casida, M. E.; Jamorski, C.; Casida, K. C.; Salahub, D. R. *J. Chem. Phys.* **1998**, *108*, 4439.

(17) Becke, A. D. *J. Chem. Phys.* **1993**, *98*, 5648.

(18) Lee, C.; Yang, W.; Parr, R. G. *Phys. Rev. B* **1988**, *37*, 785.

(19) (a) Domingo, L. R.; Picher, M. T.; Zaragozá, R. J. *J. Org. Chem.* **1998**, *63*, 9183. (b) Shukla, M. K.; Leszczynski, J. *Int. J. Quantum Chem.* **2005**, *105*, 387.

(20) (a) Halls, M. D.; Schlegel, H. B. *Chem. Mater.* **2001**, *13*, 2632. (b) Zhang, J.; Frenking, G. *J. Phys. Chem. A* **2004**, *108*, 10296. (c) Zhang, J.; Frenking, G. *Chem. Phys. Lett.* **2004**, *394*, 120. (d) Gahungu, G.; Zhang, J. *J. Mol. Struct.: THEOCHEM* **2005**, *755*, 19. (e) Gahungu, G.; Zhang, J. *J. Phys. Chem. B* **2005**, *109*, 17762. (f) Gahungu, G.; Zhang, J. *Chem. Phys. Lett.* **2005**, *410*, 302.

(21) Ahlrichs, R.; Bär, M.; Häser, M.; Horn, H.; Kölmel, C. *Chem. Phys. Lett.* **1989**, *162*, 165.

(22) Kim, Y.; Lim, S.; Kim, H. J.; Kim, Y. *J. Phys. Chem. A* **1999**, *103*, 617.

(23) Brillouin, L. *C. R. Acad. Sci.* **1934**, *46*, 618.

(24) Forés, M.; Duran, M.; Solà, M.; Adamowicz, L. *J. Phys. Chem. A* **1999**, *103*, 4413.

(25) Guallar, V.; Moreno, M.; Lluch, J. M.; Amat-Guerri, F.; Douhal, A. *J. Phys. Chem.* **1996**, *100*, 19789.

(26) Jena, N. R.; Mishra, P. C. *J. Phys. Chem. B* **2005**, *109*, 14205.

(27) AI-Ansari, I. A. Z. *J. Lumin.* **1997**, *71*, 83.

(28) Das, S. K.; Bansal, A.; Dogra, S. K. *Bull. Chem. Soc. Jpn.* **1997**, *70*, 307.

(29) Mosquera, M.; Penedo, J. C.; Ríos-Rodríguez, M. C.; Rodríguez-Prieto, F. *J. Phys. Chem.* **1996**, *100*, 5398.

(30) Kasha, M.; Heldt, J.; Gormin, D. *J. Phys. Chem.* **1995**, *99*, 7281.

(31) Santos, L.; Vargas, A.; Moreno M.; Manzano, B. R.; Lluch, J. M.; Douhal, A. *J. Phys. Chem. A* **2004**, *108*, 9331.

(32) Wanko, M.; Garavelli, M.; Bernardi, F.; Niehaus, T. A.; Frauenheim, T.; Elstner, M. *J. Chem. Phys.* **2004**, *120*, 1674.